LUNAR SURFACE CHARGING:
A GLOBAL PERSPECTIVE USING LUNAR PROSPECTOR DATA

Timothy J. Stubbs[1], Jasper S. Halekas[2], William M. Farrell[1], and Richard R. Vondrak[1]

[1]Solar System Exploration Division, NASA Goddard Space Flight Center, Greenbelt, MD 20771, U.S.A.
[2]Space Sciences Laboratory, University of California, Berkeley, CA 94720, U.S.A.
Email:Timothy.J.Stubbs.1@gsfc.nasa.gov

ABSTRACT

The electrostatic charging of the lunar surface is caused by its interaction with the local plasma environment and solar UV and X-ray induced photoemission of electrons. Probe equations are used here to calculate electrostatic lunar surface potentials as a function of angle from the subsolar point, thus giving a global perspective on charging processes. Since the Moon is in the solar wind plasma flow for most of its orbit, surface potentials are first determined for typical fast and slow stream conditions. They are then calculated using data from the Electron Reflectometer aboard Lunar Prospector. The latter reveals how the hot tenuous plasma of the lunar wake drives large negative surface potentials (up to −200 V) on the nightside of the Moon. Lunar surface charging in the Earth's magnetosphere is also discussed, with initial predictions indicating that the nightside charges to ~ −600 V in the plasma sheet. The ability to predict surface potentials is vital for understanding the lunar environment; in particular, processes such as ion sputtering and electrically-driven dust transport. The latter is especially important since dust significantly interfered with Apollo exploration activities.

1. INTRODUCTION

The surface of the Moon, like any object in a plasma, charges to an electrostatic potential that minimizes the total incident current [1]. The charging currents come from four main sources: photoemission of electrons (J_{ph}), plasma electrons (J_e), plasma ions (J_i), and secondary electrons (J_{sec}). (J_{sec} arises primarily from surface ionization by plasma electrons.) The lunar dayside typically charges positive, since J_{ph} usually dominates (see Fig. 1). As a result a "photoelectron sheath" forms above the surface, which in the solar wind extends ~1 m, and effectively shields the charged surface from the surrounding plasma [2]. On the nightside, the lunar surface usually charges negative since J_e typically dominates. In this case a "Debye sheath" shields the surface potential [3] and can extend from meters to possibly ~1 km above the surface [4]. However, there are significant uncertainties in lunar surface charging processes, and very little is known about either spatial or temporal variations.

Surface charging processes are thought to drive the transport of lunar dust grains with radii <10 μm, particularly near the terminator [5,6]. The Surveyor landers observed ≈5 μm grains levitating ~10 cm above the surface [7,8]. During the Apollo missions 0.1 μm-scale dust in the lunar exosphere was observed up to ~100 km altitude [9,10,11]. The most viable mechanisms proposed to explain these observations have been based on the principle that the like-charged surface and dust grains act to repel each other such that dust is lifted away from the surface. Under certain conditions, the heavier grains are predicted to electrostatically levitate near the surface [3,12], while the smaller grains are electrostatically "lofted" to ~10km in altitude [5,13,14]. These phenomena could present a significant hazard to future robotic and human exploration of the Moon [6,15,16].

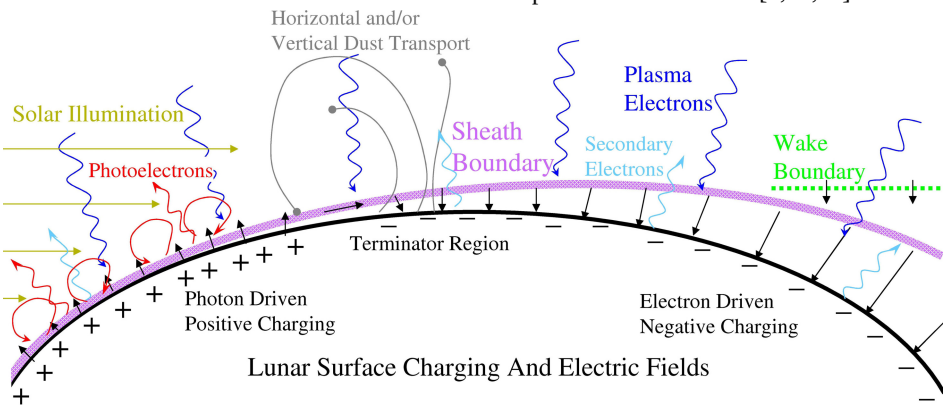

Figure 1. Schematic of the lunar electrostatic environment in the solar wind (not to scale).

Our objective here is to determine the global scale variation of electrostatic potentials and electric fields on the surface of the Moon. The electrostatic surface potentials are calculated using the probe equations from [17]. We first focus on typical fast and slow solar wind conditions, before using moments of the electron distribution function derived from Lunar Prospector Electron Reflectometer (LP/ER) data [18]. Also discussed is lunar surface charging in the magnetosphere, in particular during the Moon's traversals through the plasma sheet.

2. SPACECRAFT AND INSTRUMENTATION

The LP spacecraft was in a rapidly precessing polar orbit about the Moon (period ≈2 hours), which gave full coverage of the lunar surface twice every lunation. LP collected data for 18 months, with its altitude varying between 20 and 115 km, thus providing good coverage under most conditions. ER data is used to calculate electron concentrations (n_e) and temperatures (T_κ) from kappa fits to the electron distribution functions [18,19]. The electron kappa temperatures are converted to Maxwellian temperatures (T_e) assuming that $\kappa \approx 4.5$. Kappa and Maxwellian temperatures are related by the following equation:

$$T_e = \left(\frac{\kappa - \frac{3}{2}}{\kappa} \right) T_\kappa \approx \tfrac{2}{3} T_\kappa \qquad (1)$$

Since there is no ion data available, we assume that the plasma environment at the orbit of LP is quasi-neutral and that the electrons and ions have the same temperature, i.e., $n_i = n_e$ and $T_i = T_e$.

3. SURFACE CHARGING MODEL

We calculate the electrostatic surface potential, ϕ_S, using the method and equations given in [17]. We solve numerically to find ϕ_S such that the net incident current is approximately zero, i.e., $J_e + J_i + J_{ph} \approx 0$. ($J_{sec}$ is not included here since for solar wind conditions it is expected to be less significant than either J_e, J_i or J_{ph}, as argued by [3].) The current density equations are different for positive ($\phi_S > 0$) and negative ($\phi_S < 0$) surface potentials [e.g., see appendix in 17]. On the lunar dayside in the solar wind, we use the charging equations for a flowing plasma (most significant for J_i); while on the nightside, we use the equations for a static plasma. Photocurrent density from normally incident sunlight is assumed to be 4.0×10^{-6} A m^{-2} [20] (given a surface photoelectron emission efficiency of 0.1). J_{ph} varies with the angle from the subsolar point, θ, and so is highest at the equator at local noon ($\theta = 0°$) and drops off to zero at the terminator ($\theta = 90°$). The Debye lengths, λ_D, used in this model are for the species attracted to the surface (e.g., where $\phi_S > 0$ we use the electron Debye length). It is important to note that the dominant source of electrons over most of the lunar dayside is from photoemission (at ~100 cm^{-3} this is ~10 times greater than in the solar wind). Assuming 1-D Debye shielding above a plane, the vertical lunar surface electric field is simply given by $E_S = \phi_S / \lambda_D$.

4. MODEL PREDICTIONS

4.1 Fast and slow solar wind conditions

Solar wind flow can be broadly divided into two main types: fast and slow streams. The fast streams tend to be sourced from the poles of the Sun, while the slow streams come from the equatorial regions [21]. Fig. 2 shows predictions for ϕ_S and E_S as a function of θ, given the typical fast and slow stream solar wind conditions shown in Table 1. As expected, charging on the dayside is photo-driven ($\phi_S > 0$), while on the nightside it is electron-driven ($\phi_S < 0$). A variation in surface potential is seen on the dayside due to the decrease in solar illumination (and surface photocurrent), as the terminator is approached. No variation is shown past the terminator on the nightside, since there is no solar illumination and the plasma environment there is assumed to be both uniform and stationary.

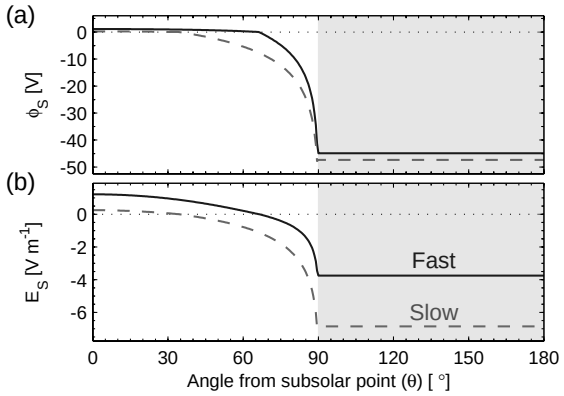

Figure 2. Lunar surface charging predictions for typical fast and slow stream solar wind conditions. Shown are (a) surface potentials, ϕ_S (V), and (b) electric fields, E_S (V m^{-1}). The grey shading indicates the lunar nightside.

Table 1. Typical fast and slow stream conditions [21].

Parameter:	Fast stream	Slow stream
n_e [cm^{-3}]	5	10
T_e [K]	1.4×10^5 (12 eV)	1.4×10^5 (12 eV)
T_i [K]	1.5×10^5 (13 eV)	1.0×10^5 (9 eV)
V_{sw} [km s^{-1}]	650	400

Interestingly, Fig. 2 also shows that on the global scale the transition from positive to negative surface potential is predicted to be well dayside of the terminator. This transition occurs at $\theta \approx 70°$ for the fast stream and $\theta \approx 35°$ for the slow stream conditions. This means that

under slow stream conditions ≈40% of the lunar surface on the dayside has a negative surface potential. We also note that the rate of change of surface potential (i.e., the electric field along the surface) is still greatest just dayside of the terminator. This result is consistent with earlier predictions by [17] and shows that under typical conditions the lunar surface just dayside of the terminator will not be positively charged, as has often been assumed. However, lunar topography near the terminator, such as mountains or crater rims, could cause an increase in the solar illumination incident on the surface, thus locally enhancing the photocurrent such that a positive surface potential could occur.

4.2 Solar wind observations from Lunar Prospector

Fig. 3 shows predictions for lunar surface charging given (a) n_e and (b) T_e derived from LP/ER data as a function of θ. On the dayside, $n_e \approx 7$ cm^{-3} and $T_e \approx 12$ eV, and so the predicted values for ϕ_S and E_S are consistent with those shown in Fig. 2 for the fast and slow solar wind streams. However, nightside of the terminator the plasma conditions vary significantly from the previous results discussed in section 4.1. As the anti-subsolar point (θ = 180°) is approached, n_e decreases rapidly while T_e increases. This variation is caused by the lunar wake.

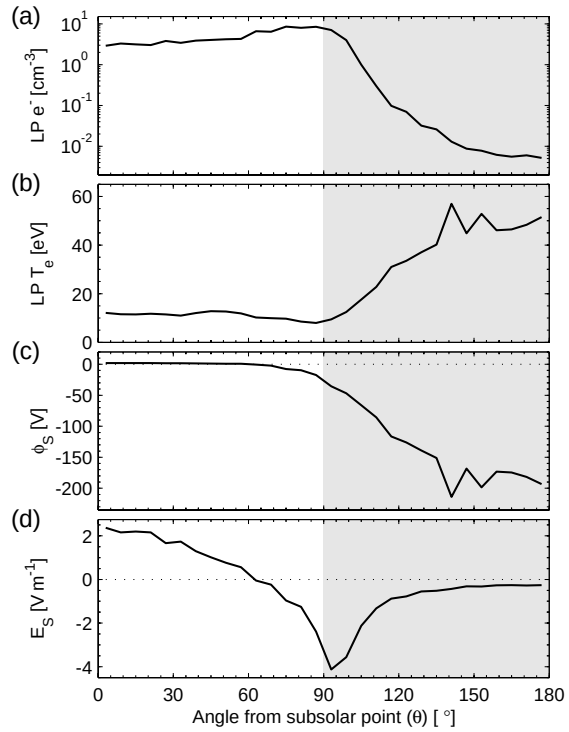

Figure 3. Lunar surface charging predictions based on LP/ER data in the solar wind. Shown are observations of (a) electron concentration, n_e (cm^{-3}) and (b) electron Maxwellian temperature, T_e (eV); and predictions for (c) surface potential, ϕ_S and (d) electric field, E_S.

On the global scale the Moon is effectively an unmagnetised dielectric body, therefore its interaction with the supersonic solar wind flow forms a void or "wake" in the antisunward direction [22]. The thermal motion of the solar wind particles allows them to fill in the wake from the flanks [23]. For any given temperature, the thermal velocity of the electrons is significantly greater than that of the ions due to the smaller electron mass. Therefore, it is the electrons that lead the infilling of the wake (note that the differential motion of the electrons and ions generates an ambipolar electric field at the terminator [6,23]). The number of electrons with sufficient energy to reach the centre of the wake (i.e., θ = 180° at the surface) decreases exponentially [19], which explains the trend in Fig. 3a. Since it is only the most thermally energetic electrons that can make it deep into the wake, this causes an increase in ambient T_e [19], as seen in Fig. 3b. Note that this increase in T_e toward the center of the wake is caused by the suprathermal tail of the solar wind electron distribution (described by the kappa function), and would not occur if it were truly Maxwellian [19].

Fig. 3c reveals that this increase in T_e in the wake results in surface potentials of up to almost −200 V. The decrease in n_e and increase in T_e also results in a significant increase in λ_D at the surface. In turn, this leads to a much weaker E_S, as shown in Fig. 3d.

4.3 The Moon in the Earth's magnetosphere

It is important to realize that the Moon is not always in the solar wind, as indicated in Fig. 4. For about one-quarter of its orbit, the Moon is either in the tenuous plasma of the magnetospheric tail lobes, or the turbulent and energetic plasmas encountered in the geomagnetic plasma sheet and magnetosheath. At the orbit of the Moon, the plasma conditions in the magnetosheath are not significantly different from those in the solar wind. However, inside the magnetosphere, the plasma environments are typically much more tenuous and significantly hotter than the solar wind. Since the geomagnetic plasma sheet is much hotter than the tail lobes, which is an important factor for surface charging, we limit our discussion here to that region.

Practically no variation was observed in n_e and T_e as function of θ when LP was in the plasma sheet. Given this apparent lack of dependence on θ, we assumed that the plasma flow, $V \approx 0$. On average, it was found that $n_e \approx 0.016$ cm^{-3} and $T_e \approx 1.9 \times 10^6$ K (161 eV) in the plasma sheet. For these observations, initial predictions indicate that on the dayside $\phi_S \approx +10$ V and E_S can be as large as +12 V m^{-1}, while on the nightside $\phi_S < -600$ V and $E_S \approx -1$ V m^{-1}. These predictions are for average conditions, which suggests that during periods of enhanced geomagnetic activity, lunar surface potentials could be much greater.

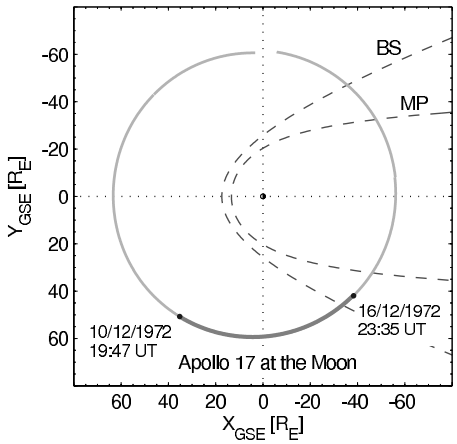

Figure 4. The Moon's orbit about the Earth during the Apollo 17 mission. View is from above the north pole with the Sun to the left. Also shown are empirical models of the Earth's bow shock, BS, and magnetopause, MP, boundaries.

5. DISCUSSION AND CONCLUSIONS

The calculations for the predictions shown in Fig. 2 and Fig. 3 only consider the vertical component of the surface electric field. Horizontal electric fields will form between regions of different surface potential, and we would expect them to be most significant near the terminator, where $d\phi_S/d\theta$ is predicted to be greatest (see Fig. 2 and Fig. 3). It is likely that these horizontal electric fields caused the enhancement in horizontal dust transport observed in-situ by the Apollo 17 LEAM experiment near the terminators [24,25].

As mentioned in section 3, we have neglected secondary electron currents, since they are not expected to be significant under solar wind conditions. However, in the hotter plasma environments of the lunar wake ($T_e \approx$ 50 eV) and the plasma sheet ($T_e \approx$ 160 eV), J_{sec} may play a much greater role in surface charging processes.

In summary:

- Lunar surface charging can vary significantly with changes in solar wind n_e, T_e, T_i and V_{sw}, as shown in Fig. 2, with variations in n_e and T_e being particularly important.
- The lunar wake plays a major role in the charging of the lunar nightside in the solar wind, as shown in Fig. 3. This is due to the exponential drop in n_e and increase in T_e toward the centre of the wake. On average, we predict nightside surface potentials of up to −200 V.
- Lunar surface charging is considerably different in the magnetosphere than in the solar wind. For example, in the plasma sheet surface potentials are predicted to be much greater, especially on the lunar nightside (~ −600 V).

The results presented here have begun to reveal the global scale variations in lunar surface charging and the strong dependence on the ambient plasma conditions in the solar wind or magnetosphere.

6. REFERENCES

1. Whipple, E.C., *J. Geophys. Res.*, 1525, 1977.
2. Singer, S.F. and Walker, E.H., *Icarus*, 1, 7, 1962.
3. Nitter, T. et al., *J. Geophys. Res.*, 6605, 1998.
4. Halekas, J.S., et al., *Geophys. Res. Lett.*, 2003GL018421, 2003.
5. Stubbs, T.J., et al., A dynamic fountain model for dust in the lunar exosphere, *Proc. Dust Planet. Sys.*, submitted, 2006.
6. Stubbs, T.J., et al., Impact of dust on lunar exploration, *Proc. Dust Planet. Sys.*, submitted, 2006.
7. Criswell, D.R., *Photon & Particle Interactions with Surfaces in Space*, 545, 1973.
8. Rennilson, J.J. and Criswell, D.R., *The Moon*, 10, 121, 1974.
9. McCoy, J.E. and Criswell, D.R., *Proc. Lunar Sci. Conf. 5th*, 2991, 1974.
10. McCoy, J.E., *Proc. Lunar Sci. Conf. 7th*, 1087, 1976.
11. Zook, H.A. and McCoy, J.E., *Geophys. Res. Lett.*, 18, 2117, 1991.
12. Sickafoose, A.A. et al., *J. Geophys. Res.*, 2002JA009347, 2002.
13. Stubbs, T.J., et al., *Adv. Space Res.*, in press, 2005.
14. Stubbs, T.J., et al., *Lunar Planet. Sci. Conf. 36th*, 1899, 2005.
15. *NASA Robotic and Human Lunar Exploration Strategic Roadmap* (2005).
16. Stubbs, T.J., et al., *Lunar Planet. Sci. Conf. 36th*, 2277, 2005.
17. Manka, R.H., *Photon & Particle Interactions with Surfaces in Space*, 347, 1973.
18. Halekas, J.S., et al., *Geophys. Res. Lett.*, 2001GL014428, 2002.
19. Halekas, J.S., et al., *J. Geophys. Res.*, 2004JA010991, 2005.
20. Goertz, C.K., *Rev. Geophys.*, 27, 271, 1989.
21. Hundhausen, A.J., The solar wind, *Introduction to Space Physics*, Cambridge Univ. Press, 1995.
22. Ogilvie et al., *Geophys. Res. Lett.*, 23, 1255, 1996.
23. Farrell et al., *J. Geophys. Res.*, 103, 23653, 1998.
24. Berg, O.E., et al., *Interplanetary Dust and Zodiacal Light*, 233, 1976.
25. Berg, O.E., Earth Planet. Sci. Lett., 39, 377, 1978.